Construction and Building Materials 492 (2025) 142996

Contents lists available at ScienceDirect

Construction and Building Materials

journal homepage: www.elsevier.com/locate/conbuildmat

Surface treatment of waste tire rubber via oxidation and alkalization for enhanced compatibility with bitumen

Nie Tian [a,*], Piergiorgio Tataranni [a], Yinzhang He [b], Cesare Sangiorgi [a]

[a] Department of Civil, Chemical, Environmental, and Materials Engineering, University of Bologna, Via Umberto Terracini 28, Bologna, BO 40131, Italy
[b] School of Highway, Chang'an University, Xi'an 710000, China

ARTICLE INFO

Keywords:
Waste tire recycling
Asphalt pavement
Compatibility
Surface treatment
Hydrogen peroxide
Sodium hydroxide

ABSTRACT

The accumulation of waste tires poses critical environmental and engineering challenges. Incorporating waste crumb rubber (WCR) into asphalt pavements enhances recycling and pavement performance, yet limited compatibility between WCR and bitumen remains a constraint. This study explores surface treatments using hydrogen peroxide (H_2O_2) and sodium hydroxide (NaOH) under varying intensities. Microscopic analysis (scanning electron microscopy (SEM), specific surface area (SSA), contact angle, and Fourier transform infrared (FTIR) spectroscopy) and macroscopic evaluations (striping rates by modified boiling test) on coarse WCR, and storage stability test on rubberized binders reveal that both treatments enhance interfacial adhesion and compatibility through surface etching and polar group incorporation. Within 2 mol/L, H_2O_2 treatment becomes increasingly effective with higher concentration and temperature, whereas NaOH solutions exceeding 15 % at elevated temperatures cause excessive corrosion without further interfacial improvement. Unexpectedly, both treatments may induce the micro-swelling effect, modifying WCR viscoelasticity, with NaOH exhibiting a more pronounced impact.

1. Introduction

The disposal of end-of-life tires poses an ongoing environmental and public health concern, encompassing extensive land occupation, potential fire hazards, soil and water contamination, while also creating favorable conditions for disease vector proliferation [28,31,38]. Among various recycling strategies, incorporating ground rubber into asphalt pavements gained attention as a practical and efficient means while enhancing pavement performance to some extent. This dual benefit renders it a promising approach from both environmental and economic perspectives [4,9].

Waste crumb rubber (WCR) can be incorporated through the dry process (CRdry), wet process (CRwet), and terminal blending (CRtb) [13]. In CRdry, WCR up to around 4 mm is used to partially replace mineral aggregates or fine sand in asphalt mixtures, offering low cost, simplicity, and high recycling efficiency while improving fatigue resistance and impact absorption [19,8]. In contrast, the CRwet process involves blending bitumen at approximately 180 °C with 10–30 % WCR powder to produce the rubberized binder [3]. CRtb, fundamentally similar to CRwet, modifies asphalt binders rather than mixtures but requires specialized equipment to ensure complete WCR digestion at temperatures almost exceeding 200 °C [17,36]. Both CRwet and CRtb employ high temperature and shear to enhance WCR-bitumen interaction. During this process, WCR absorbs light fractions from bitumen and undergoes swelling, which reduces its surface elasticity and increases its viscous behavior [32]. This transformation partially disrupts the cross-linked network of WCR, loosens the structure, and releases embedded fillers like carbon black. The resulting porosity facilitates bitumen penetration and interdiffusion, while the softened surface lowers interfacial tension and elastic recoil. These changes improve wetting, interfacial adhesion, and physical interlocking, thereby enhancing the compatibility and stability of the WCR-bitumen system, with benefits for pavement cracking and rutting resistance [14,24]. Despite current studies providing a solid theoretical foundation and practical insights into WCR recycling in pavements, these technologies still face distinct technical bottlenecks and engineering constraints that limit their performance consistency and broader implementation.

In more detail, in CRdry, WCR undergoes rapid initial swelling upon contact with bitumen, particularly in hot mixture applications. Elevated temperatures intensify the swelling rate and extent, which can lead to

* Corresponding author.
E-mail addresses: nie.tian2@unibo.it (N. Tian), piergiorg.tataranni2@unibo.it (P. Tataranni), heyinzhang@chd.edu.cn (Y. He), cesare.sangiorgi4@unibo.it (C. Sangiorgi).

https://doi.org/10.1016/j.conbuildmat.2025.142996
Received 9 May 2025; Received in revised form 13 July 2025; Accepted 1 August 2025
Available online 9 August 2025
0950-0618/© 2025 The Authors. Published by Elsevier Ltd. This is an open access article under the CC BY license (http://creativecommons.org/licenses/by/4.0/).

uncontrolled volume expansion during mixing and compaction [32]. This inevitable expansion induced by the swelling effect, combined with the inherently weaker adhesion of WCR to bitumen compared to mineral aggregates, may compromise the volumetric stability and internal cohesion of the mixture. Practically, this can translate into construction difficulties like mixture segregation and inconsistent workability, and ultimately, premature deterioration in the field, manifesting as moisture damage, raveling, and stripping. In CRwet, WCR is first blended with hot bitumen to allow partial interaction before mixing with aggregates. While this process improves compatibility to some degree by enhancing diffusion and swelling, the chemical reactivity between bitumen and the crosslinked rubber network remains limited, often resulting in insufficient bonding and storage instability due to incomplete integration. Moreover, the density disparity between WCR and bitumen drives phase separation during storage and application, especially when storage time is prolonged or temperature fluctuates [20]. CRtb, which integrates WCR into bitumen at the refinery or production plant under controlled conditions, offers better processing consistency. However, it is also sensitive to temperature, mixing duration, and material composition. Also, the chemical inertness of vulcanized WCR limits deeper molecular interactions with bitumen. These constraints hinder uniform dispersion and lead to performance variability in the field. Collectively, despite their methodological differences, all three approaches suffer from a fundamental issue: the inherent incompatibility between WCR and bitumen. Then, poor bonding, insufficient wetting, and limited interfacial interactions impede both the durability of binder systems in wet processes and the quality of mixtures in dry processes.

Based on the above, surface treatment for WCR has emerged as a key research focus to enhance its compatibility with bitumen by modifying the physical and chemical properties of the outer layer. Early methods primarily involved mechanical grinding and high-temperature pyrolysis, while advancements in machinery and technology have introduced plasma treatment, ultraviolet irradiation, microwave processing, biodegradation, oxidation, grafting, and even composite methods. Among these, chemical reagent-based approaches have gained widespread adoption due to their effectiveness, operational simplicity, and minimal equipment requirements. However, many chemical reagents pose significant toxicity and environmental risks during use and disposal. In particular, organic compounds such as octadecylamine (ODA) [7], toluene-2,4-diisocyanate (TDI) [33], acrylamide [35], and styrene [41] can adversely affect human skin, eyes, the respiratory system, internal organs, and the nervous system. Improper handling or disposal may lead to soil and water contamination, contradicting the fundamental goal of environmental sustainability in waste tire recycling. To address these concerns, this study adopts oxidation and alkalization surface treatments using hydrogen peroxide (H_2O_2) and sodium hydroxide (NaOH), carefully balancing economic feasibility, operational efficiency, and industrial accessibility. These treatments are applied as a pre-treatment step before the dry or wet process. Moreover, the disposal and treatment of H_2O_2 and NaOH waste solutions are mature and widely used in related industries, ensuring environmental compliance.

Regarding the oxidation reagents in more detail, H_2O_2 and ozone, as the most common oxidizers in the liquid and gas phases, can alter the molecular structure of WCR by breaking chemical bonds and introducing additional polar functional groups, which enhance surface roughness and reactivity, thereby improving WCR adhesion and compatibility with bitumen [18,23,40]. Ozone treatment, however, requires complex production equipment and higher costs. In contrast, H_2O_2 is readily available and can exert strong oxidative effects through simple pH adjustment and catalyst activation. As reported by Li et al. [18], Memon's study was among the first to apply H_2O_2 for surface treatment of WCR, laying a foundation for oxidative activation. Building on this, Shatanawi et al. [26] introduced a Fenton system by adding Fe^{2+} as a catalyst to H_2O_2 treatment, which promoted hydroxyl radical (·OH) generation and accelerated degradation of the vulcanized structure. In a follow-up study, Yu et al. [39] applied X-ray photoelectron spectroscopy (XPS) to analyze the compatibility enhancement with the increase of polar functional groups such as hydroxyl (-OH) and carbonyl (C═O), and further investigated how oxidation conditions influenced the interfacial compatibility through bitumen performance tests. Li et al. [16] examined the microstructural characteristics of H_2O_2-activated WCR and its effects on the rheological properties of the modified bitumen. Sun et al. [29] evaluated the water stability of H_2O_2-treated WCR-modified asphalt mixtures through freeze-thaw tests. However, most previous studies focused more on evaluating the performance of rubberized binder, with limited direct characterization of changes in WCR itself. This narrows their relevance for applications in the dry process, where WCR's surface properties are critical. To address this gap, our previous work systematically investigated the activation effects of H_2O_2 on WCR through microscopic and macroscopic analyses, as well as molecular dynamics simulations [30]. Nonetheless, comparative analyses across varying treatment intensities remain limited, underscoring the need for a more comprehensive understanding of WCR surface evolution and interfacial behavior.

As a typical strong alkali, NaOH can directly hydrolyze and etch the WCR surface without requiring a catalyst, thereby increasing surface reactivity. More importantly, it facilitates the dissolution and removal of metal compounds, particularly zinc oxides and zinc stearates, through saponification or complexation reactions. This not only improves surface cleanliness but also reduces the potential environmental risks associated with zinc leaching during subsequent asphalt applications [11]. Nuzaimah et al. [22] reported that within a 10 % NaOH solution, higher concentration leads to increased surface roughness and a greater introduction of polar functional groups. [21] and Si et al. [27] indirectly demonstrated the role of NaOH in enhancing WCR's surface polarity and interfacial activity by analyzing the reduction of air voids and the improvement in bond strength in rubberized concrete. Notably, due to prolonged exposure to light, heat, and oxidation during service, WCR already contains a certain amount of polar functional groups. However, these groups readily dissociate upon reacting with NaOH, increasing surface charge density and thus exhibiting greater polarity [6]. Overall, NaOH surface treatment also proves to be highly effective for WCR. Nevertheless, existing research has predominantly focused on its application in cement concrete [1,12,2,25], while its potential to improve WCR-bitumen interfacial compatibility and its applicability in asphalt mixtures remains further investigated.

This study applies H_2O_2 and NaOH solutions to modify the surface of WCR in different particle sizes and shapes, with treatment intensities categorized as mild, moderate, and severe. To evaluate the treatment effects, coarse WCR samples were analyzed using scanning electron microscopy (SEM), specific surface area (SSA) analysis, contact angle testing, and Fourier transform infrared (FTIR) spectroscopy to examine surface morphology, wettability, and chemical composition changes. Additionally, a modified boiling test was conducted at the macroscopic scale to directly assess WCR-bitumen adhesion. Fine WCR was used for the preparation of rubberized binder, where storage stability testing was employed to indirectly evaluate the compatibility. The research framework is illustrated in Fig. 1. This study investigates the effects of two environmentally friendly reagents on WCR surface treatment, providing insights for optimizing treatment conditions and challenging conventional assumptions regarding the correlation between reaction intensity and treatment effectiveness.

2. Materials and experimental methods

2.1. Materials

The materials used in this study primarily include WCR of various shapes and sizes, chemical reagents for surface treatment, and two types of bitumen designated for the modified boiling test and storage stability tests.

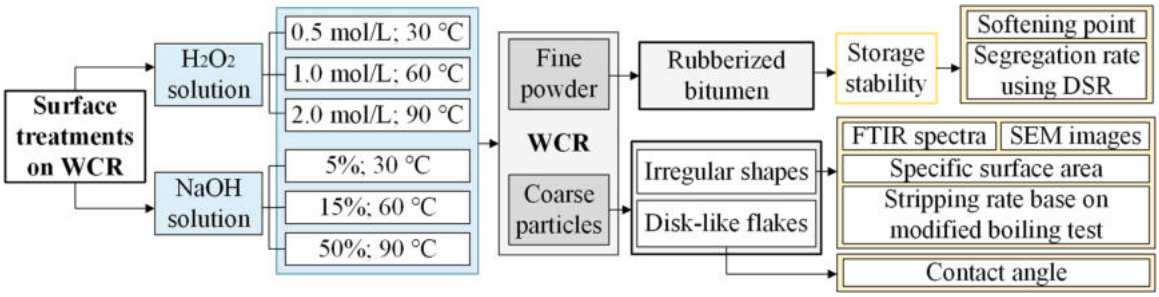

Fig. 1. Framework of the research work.

2.1.1. WCR

The WCR used in this study was supplied by Genan S.A. (Portugal) and was processed through a granulation process at ambient temperature from end-of-life tires, as shown in Fig. 2. The chemical abstracts service registry numbers (CAS NR) and the corresponding composition of its main constituents are listed in Table 1. To meet different experimental requirements, WCR was sieved and classified into two sizes. The coarse WCR, measuring 4.0–5.0 mm, was used for direct characterization of surface morphology and chemical composition changes, including SEM testing, FTIR spectroscopy analysis, SSA measurement, and modified boiling test. The fine WCR of 0.5–1.0 mm was for preparing rubberized binder, with phase separation analysis employed to indirectly evaluate WCR-bitumen compatibility. Additionally, to meet the specific requirements of contact angle measurements, cylindrical WCR samples with a diameter of 8 mm and a height of 2 mm were prepared.

2.1.2. Chemical reagents for surface treatments

For H_2O_2-based treatment, a 30 % H_2O_2 solution was diluted with deionized water to different concentrations: 0.5 mol/L, 1 mol/L, and 2 mol/L. To enhance the catalytic activity of the Fenton reaction, 1 % $FeSO_4{\cdot}7\ H_2O$ was added to each solution as a catalyst, and the pH was adjusted to 3 using 2 mol/L HCl.

For NaOH-based treatment, NaOH crystals were dissolved in deionized water to prepare solutions with concentrations of 5 %, 15 %, and 50 %. This method does not require additional catalysts or pH adjustments during the surface treatment process.

During the experimental validation phase, two types of bitumen were used after the WCR surface treatment. The performance parameters of them are detailed in Table 2 and Table 3. One was 50/70 neat bitumen, utilized for the preparation of rubberized binder and storage stability test. The other was a polymer-modified emulsion (PmE), employed in the modified boiling test.

2.2. Sample preparation

2.2.1. Surface treatment on WCR

Three kinds of WCR were subjected to surface treatment using two methods, each with three intensity levels. Table 4 presents the sample coding scheme under different test conditions. The first letter, "H" and "S", denotes the reagents H_2O_2 and NaOH, respectively. The middle letter, "L", "M", and "H", represents the treatment intensity (low, medium, and high), while the last letter, "F", "C", and "D", indicates the WCR morphology (fine powder, coarse particles, and disk-like flakes). The treatment duration under each designed experimental condition was set

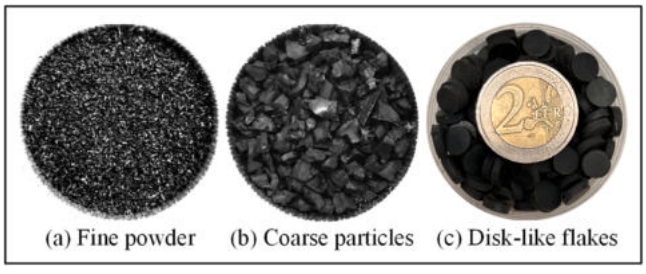

Fig. 2. WCR samples for surface treatments.

Table 1
Main components and contents of WCR.

Components	CAS NR	Content (%)	Notes
Natural rubber (NR)	/	76.3	/
Vulcanizing agents	1569–69–3	1.2	May contain thiol structures
Mineral oil	/	4.3	/
Dicyclohexane	101–83–7	0.1	/
Oleic acid	112–80–1	0.4	/
Stearic acid	57–11–4	1.2	/
N-(1,3-Dimethylbutyl)-N′-phenyl-p-phenylenediamine	793–24–8	3.0	/
Zinc oxide	1314–13–2	1.5	/
Calcium sulphate	7778–18–9	0.5	Possibly contains calcium carbonate
Carbon black	1333–86–4	5.7	/
Silicon dioxide	14808–60–7	5.8	/

Table 2
Typical values of 50/70 neat bitumen.

Properties	Units	Values		Methods
		Min	Max	
Penetration at 25 °C	1/10 mm	50	70	EN 1426
Softening point, Ring & Ball	°C	46	54	EN 1427
Penetration index	-	−1.5	0.7	EN 12591
Fraass breaking point	°C		−8	EN 12593
Relative density at 25/25 °C	-	1.00	1.10	EN ISO 3838
Flash point, COC	°C	250		EN ISO 2592
Dynamic viscosity at 60 °C	Pa·s	145		EN 12596
Ductility	%	80		ASTM D 113
Solubility in organic solvents	% (m/m)	99.0		EN12592
Resistance to aging (RTFOT):	-			EN 12607–1
-Mass change (absolute value)	%		0.5	
-Residual penetration at 25 °C	%	50		EN 1426
- Increase in softening point	°C		9	EN 1427

Table 3
Typical values of SBS-modified emulsion.

Properties	Units	Values	Methods
Binder content	%	63–67	EN 1428
Breaking index	-	70–155	EN 13075–1
Viscosity at 40 °C (cup discharge time 4 mm)	sec	5–70	EN 12846
Adhesiveness	%	≥ 90	EN 13614
Penetration at 25 °C	dmm	45–80	EN1426
Softening point	°C	≥ 60	EN1427

Table 4
Sample code of the WCR after surface treatment.

Conditions		Surface treatment on WCR						Rubberized binders	
		Fine		Coarse		Disk-like			
H_2O_2	0.5 mol/L, 30 °C	H_F	HLF	H_C	HLC	H_D	HLD	H_FB	HLFB
	1.0 mol/L, 60 °C		HMF		HMC		HMD		HMFB
	2.0 mol/L, 90 °C		HHF		HHC		HHD		HHFB
NaOH	5 %, 30 °C	S_F	SLF	S_C	SLC	S_D	SLD	S_FB	SLFB
	15 %, 60 °C		SMF		SMC		SMD		SMFB
	50 %, 90 °C		SHF		SHC		SHD		SHFB
Control	Untreated	U_F		U_C		U_D		U_FB	

to 1 h. The detailed treatment process is illustrated in Fig. 3. Before these treatments, WCR was not pre-cleaned with any reagent. Upon completion, the waste solution was separated using fine-mesh gauze or sieves to facilitate proper waste handling, and the treated WCR was thoroughly rinsed with distilled water.

2.2.2. Preparation of rubberized binders

The rubberized binder was prepared using fine WCR. The designation of each sample is presented in Table 4. The preparation process and related conditions followed the conventional CRwet technology and the specifications of ASTM D7173, as detailed below:

(a) Heat the 50/70 penetration neat bitumen to 150 °C.
(b) Gradually add 15 % of H_FB, S_FB, or U_FB while stirring for 10 min.
(c) Maintain 180 °C shearing at 1500 RPM for 1 h to achieve mechanical homogenization.
(d) Load the rubberized binder into 25 mm diameter aluminum tubes, with each sample having a height of approximately 120 mm. The tubes were then vertically stored at 163 °C for 48 h, followed by horizontal freezing at −10 °C.

2.3. Experimental methods

The compatibility between WCR and bitumen depends on the physical and chemical properties of the WCR surface. Microscopic analyses reveal changes in surface texture, porosity, wettability, and chemical composition, providing direct evidence for compatibility and adhesion potential. Additionally, the modified boiling test assesses WCR-bitumen adhesion via bitumen S_r, while the storage stability test indirectly reflects molecular interaction intensity through the S_{diff} and S_p. To ensure the reliability and objectivity of the experimental results, tests involving a limited quantity of samples, such as SEM observation, softening point measurements, and the modified boiling test, were conducted in duplicate or triplicate. For other tests where a larger quantity of material was analyzed, where each test inherently yielded multiple data points, or where the sample already had high representativeness, parallel repeats were not separately conducted.

2.3.1. Microscopic analysis

2.3.1.1. SEM images. The surface morphology of coarse WCR samples H_C, S_C, and U_C was examined using a JEOL JSM-6010 SEM. Additionally, to preliminarily determine whether the surface treatment merely achieved surface cleaning and to distinguish between treated and pre-cleaned WCR, SEM was also conducted on acetone-cleaned WCR. The magnification range was set between 300X and 10kX. Since WCR is insulated and SEM imaging relies on electron beam scanning, a metal coating was applied to the samples before observation to ensure image quality.

2.3.1.2. SSA analysis. The Micromeritics ASAP 2460 fully automated specific surface area and porosity analyzer was used to test the coarse WCR samples. Samples underwent thorough degassing to remove surface-adsorbed moisture and volatile components before measurement. The free space in the sample cell was automatically calibrated, and the nitrogen (N_2) adsorption volume (V) was recorded at different relative pressures (P/P_0). Based on the Brunauer-Emmett-Teller (BET) theory and Eq. (1), the adsorption behavior of N_2 at 77 K was analyzed. The monolayer adsorption volume (V_m) was determined from the slope and intercept of the linear region of the adsorption isotherm. Finally, the SSA of the samples was calculated from Eq. (2).

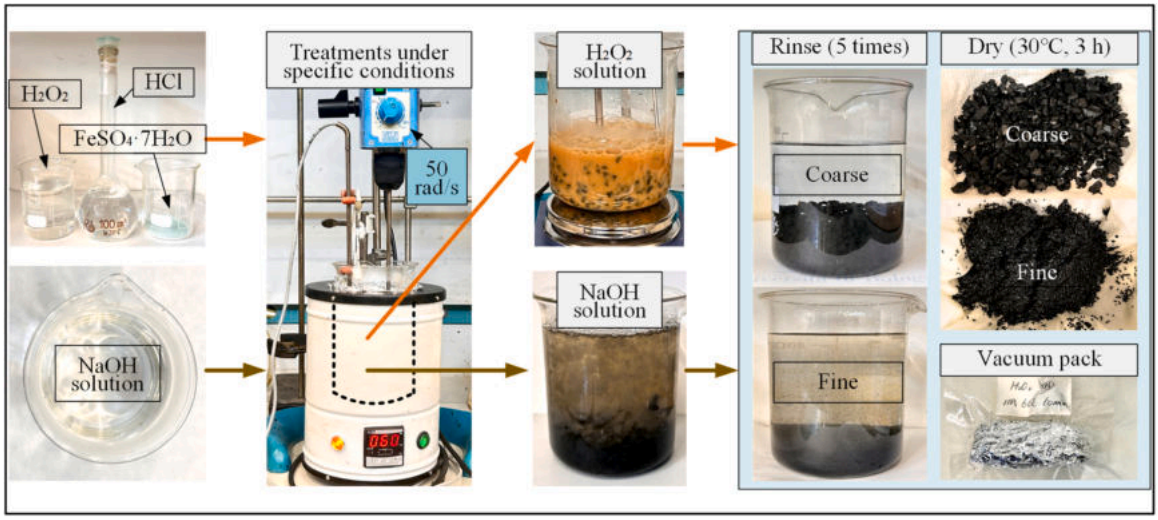

Fig. 3. Processes of the surface treatments on WCR.

$$\frac{P}{V(P_0 - P)} = \frac{1}{V_m C} + \frac{C-1}{V_m C} \bullet \frac{P}{P_0} \quad (1)$$

$$S = V_m \bullet N_A \bullet \sigma \quad (2)$$

Where V and V_m are measured in cm^3 /g. The constant C is known as the BET constant, which reflects the relative energy of adsorption for the first monolayer compared to subsequent multilayers. For the relative pressure P/P_0, P represents the equilibrium pressure of the nitrogen, and P_0 refers to the saturated vapor pressure of nitrogen at the experimental temperature. The parameter N_A refers to Avogadro's constant, which is 6.022×10^{23} molecules per mole. Lastly, σ indicates the surface area occupied by a single adsorbed nitrogen molecule in the monolayer, typically assumed to be 0.162 nm^2 for nitrogen gas.

2.3.1.3. Contact angle measurement. The contact angle of H_C, S_C, and U_C samples with distilled water at ambient temperature was measured using Lauda Scientific LSA100 produced in Germany. A droplet volume of 5 μL was dispensed onto the sample surface using a precision syringe, and the contact angle was recorded within 5 s after droplet placement to minimize evaporation effects and ensure test consistency. The contact angle indicates the hydrophilicity of WCR samples, whereas a smaller contact angle signifies stronger wettability, which is beneficial for WCR-bitumen interaction and adhesion, especially considering the use of emulsified bitumen. The contact angle results would also provide preliminary insights into the potential introduction of polar functional groups like -OH, -COOR, and S═O.

2.3.1.4. FTIR spectroscopy. FTIR spectroscopy further supported the analysis of how different reagents and concentrations influence the surface chemical composition of WCR. The measurements were performed using a Thermo Scientific Nicolet iS50 spectrometer produced in the USA. The samples included H_C, S_C, and U_C. The pressing plate method was used for sample preparation, followed by scanning the sample surface. The tests were conducted in ATR mode, with a spectral range of 4000–600 cm^{-1}. Baseline correction and peak detection were performed using OMNIC and Origin 2024b.

2.3.2. Storage stability test

Stokes' law suggests that the density difference and interfacial interactions between WCR and bitumen are key factors influencing the phase separation of rubberized binder [37]. This indicates a strong correlation between storage stability and compatibility [5]. Therefore, in this study, WCR-bitumen compatibility is indirectly analyzed based on softening point difference (S_{diff}), as defined in Eq. (3), and the segregation percentage (S_p) calculated from the complex modulus (G^*) in Eq. (4). Where, S_t and S_b denote the softening points of the top and bottom samples, respectively. G_t^*, G_b^* and G_{avg}^* represent G^* of the top, bottom, and average values of the rubberized binder specimen, respectively. The experimental procedure is illustrated in Fig. 4. For DSR testing, the frequency was set to 1.59 Hz (10 rad/s). A parallel plate configuration was used, with a 1 mm gap and a 25 mm plate diameter at 60 °C, and a 2 mm gap with an 8 mm plate diameter at 25 °C.

$$S_{diff} = |S_t - S_b| \times 100\% \quad (3)$$

$$S_p = \frac{\mathrm{Max}(G_t^*, G_b^*) - G_{avg}^*}{G_{avg}^*} \times 100\% \quad (4)$$

2.3.3. Modified boiling test

A modified boiling test was performed on coarse WCR, as shown in Fig. 5, with the stripping rate (S_r) from Eq. (5) used as the evaluation metric. Given that hot bitumen can accelerate the swelling of WCR during coating, emulsified bitumen, which exhibits better fluidity at ambient temperature, was used for WCR coating. The specific procedure is as follows:

(a) Weigh approximately 50 g of WCR samples and record the mass as m_0.
(b) Coat samples with emulsified bitumen, then dry at 30 °C for 3 h, recording the mass as m_1.
(c) Record the total mass of the beaker and the rod as m_2 and heat the water to a gentle boil.
(d) Immerse samples for 20 min, then stir for 3 min to remain detached bitumen in the container.
(e) Dry the container and record the total mass with the rod as m_3.

$$S_r = \frac{m_3 - m_2}{m_1 - m_0} \times 100\% \quad (5)$$

3. Results and discussion

3.1. Microscopic analysis

3.1.1. SEM images

Fig. 6 presents SEM images of untreated and acetone-cleaned WCR, serving as references for analyzing the treated samples. The surface of the untreated WCR shown in Fig. 6(a) exhibits an accumulation of particles of varying sizes, attributed to complex additives and impurities like residual dust. In contrast, the pre-cleaned sample in Fig. 6(b) reveals a clearer surface texture, as a significant portion of adhered debris has been dissolved or removed, resulting in a smoother and cleaner overall appearance.

In contrast, WCR treated with two chemical reagents presents distinct surface morphological features. Fig. 7(a) illustrates a progressive change in H_2O_2-treated WCR, where increasing treatment intensity results in a cleaner surface with more pores and even fissures. This phenomenon is primarily attributed to the enhanced oxidative capacity of the Fenton reaction, in which externally introduced Fe^{2+} catalyze the decomposition of H_2O_2 to produce highly reactive ·OH. These radicals initiate a cascade of oxidative attacks on the WCR surface, cleaving unsaturated C═C bonds and degrading sulfur crosslinks, while simultaneously oxidizing embedded organic residues. This aggressive surface

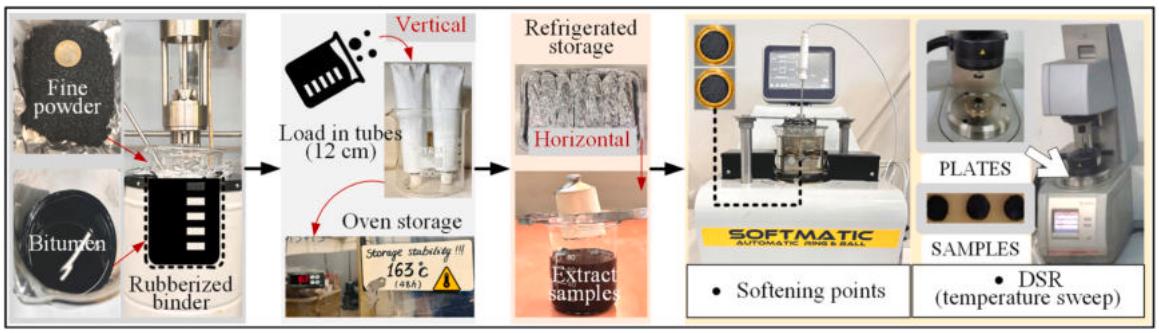

Fig. 4. The experiment process of the storage stability test.

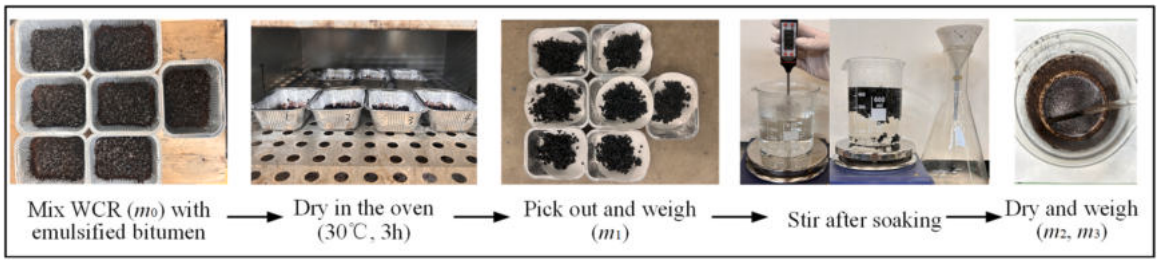

Fig. 5. The experiment process of the modified boiling test.

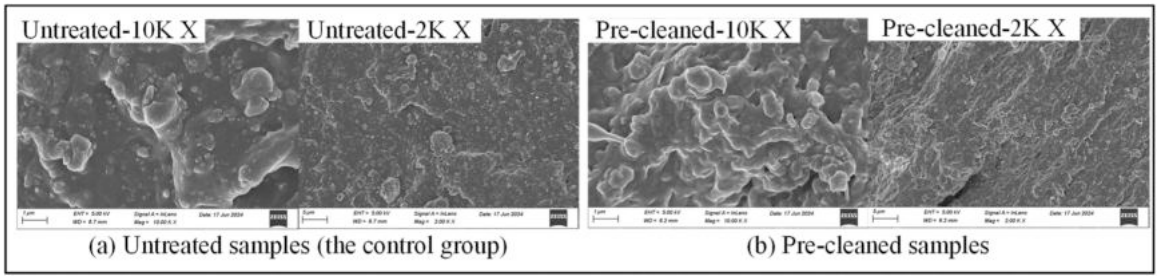

Fig. 6. SEM images of untreated and pre-cleaned WCR.

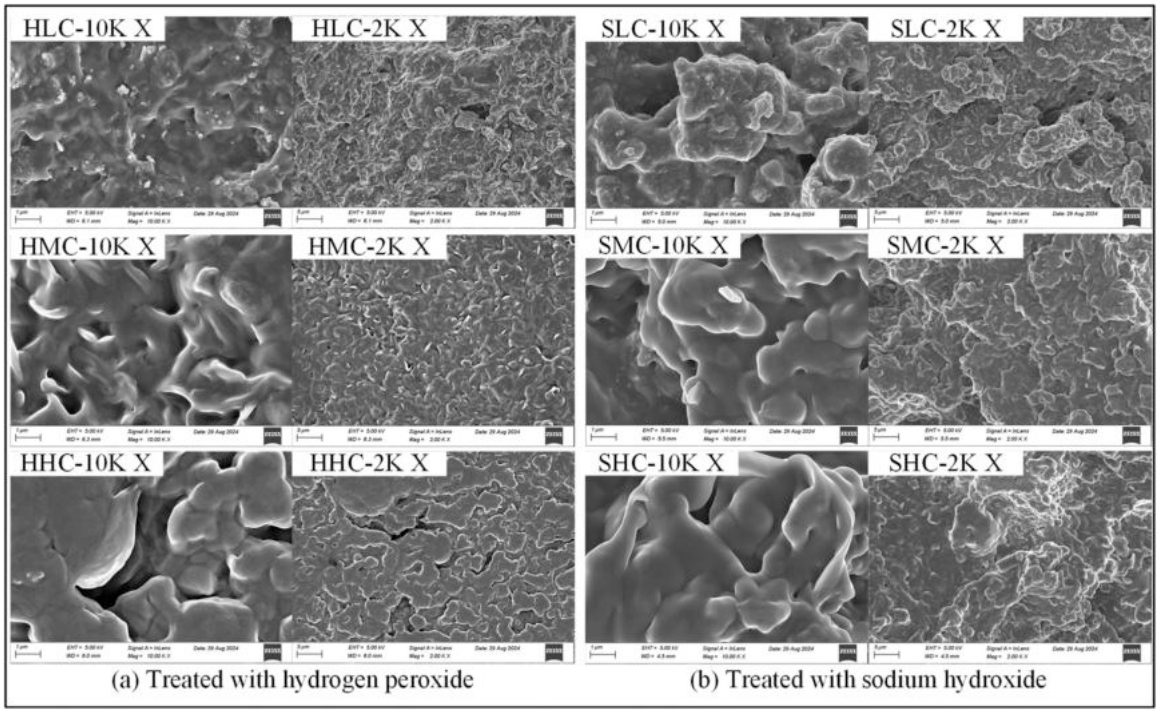

Fig. 7. SEM images of WCR treated with H_2O_2 and NaOH solutions.

activation leads to the progressive removal of obstructive layers. As a result, pronounced grooves, pores, and interconnected channels, particularly evident in the HHC sample, which resembles brain cross-sections, increase SSA and facilitate bitumen infiltration and mechanical interlocking, thereby substantially improving interfacial adhesion.

Fig. 7(b) illustrates the surface changes in NaOH-treated WCR samples. While the trend in cleanliness is similar to that observed in H_2O_2-treated samples, the enhancement in surface roughness and porosity is less pronounced. With increasing solution concentration and temperature, the WCR surface appears smoother, seemingly challenging the conventional assumption that greater treatment intensity leads to more severe surface etching. To mitigate the limitations of localized SEM observations, a more comprehensive analysis incorporating SSA measurements and FTIR spectroscopy is required for a thorough evaluation.

3.1.2. SSA analysis

Table 5 details the SSA calculation of WCR under different treatment conditions, calculated based on the BET theory. To minimize the influence of impurities in fine WCR, the tests were conducted on coarse WCR, which inherently has a lower SSA but still allows for valid comparative analysis. As a result, the HLC and HMC samples exhibited N_2 adsorption values below the instrument's detection limit, making it impossible to

Table 5
Results of specific surface area calculation.

Samples	Mass (g)	Slop $(\frac{C-1}{V_mC})$	Intercept $(\frac{1}{V_mC})$	Correlation coefficient	SSA (m^2/g)
HLC	2.26	/	/	/	below detection limit
HMC	2.30	/	/	/	below detection limit
HHC	2.30	243.23	11.66	0.9947	0.0171
SLC	2.33	250.19	8.13	0.9949	0.0168
SMC	2.32	986.81	−7.73	0.9901	0.0044
SHC	2.37	752.48	0.49	0.9954	0.0058
U_C	/	/	/	/	below detection limit

determine the SSA. Additionally, the SSA of SMC and SHC was relatively low, measured at 0.0044 m^2/g and 0.0058 m^2/g, respectively. SEM images suggest that this phenomenon is likely attributed to the collapse of microvoids and the formation of a smoother, less porous surface, induced by the swelling-dissolution effect of WCR under strong alkaline and high-temperature conditions.

HHC and SLC exhibited a significant increase in SSA, measuring 0.0171 m^2/g and 0.0168 m^2/g, respectively. The SSA of U_C was also below the detection limit, consistent with SEM images showing a surface without distinct porosity. For a more intuitive comparative analysis, assuming U_C to be a 4 mm cube, octahedron, or sphere, the theoretical SSA would be 0.0026, 0.00184, and 0.0015 m^2/g, respectively, with an average of 0.00198 m^2/g. This implies that the SSA of HHC and SLC, which exhibited the most pronounced porosity improvement, is approximately 8.5 times that of U_C. The SSA analysis aligns with SEM observations, further emphasizing that the surface etching effects in HHC and SLC samples were the most significant.

3.1.3. Contact angle measurement

WCR generally exhibits poor wettability and low surface energy, primarily due to the long-chain hydrocarbons lacking polar functional groups. Additionally, the crosslinked network formed during vulcanization, along with complex additives such as carbon black and plasticizers, further contributes to its nonpolar surface characteristics. The macro-scale observation in Fig. 8 confirms the strong hydrophobicity of untreated WCR, as evidenced by the large water droplets retained on the surface. Further experimental measurements indicate a contact angle of approximately 150°, reinforcing this hydrophobic behavior. Such characteristics hinder the initial bitumen wetting and interfacial adhesion on WCR surfaces, particularly in the dry process, where emulsified bitumen is used for asphalt mixtures. In general, the contact angle between typical tire rubber and distilled water ranges from 120° to 130° [34]. However, in this study, the pellet-shaped particles used for SEM analysis developed a new surface film during the cutting process, resulting in an increased contact angle.

Compared to the U_D, the contact angle of the treated samples decreased significantly by approximately 1/4–1/3, with all values falling within 100° to 115°, exhibiting relatively minor variations. Further observations suggest that the contact angle reduction from HLD to HMD is greater compared to that from HMD to HHD. However, the overall trends do not fully correspond to the SEM and SSA conclusions. For instance, SHD exhibits the lowest contact angle, indicating the highest wettability. This discrepancy arises because SEM and SSA primarily capture physical microstructural characteristics, whereas contact angle measurements reflect both the physical and chemical properties of the WCR surface. Nevertheless, it is worth emphasizing that both treatments (regardless of the intensity) effectively enhance surface wettability compared to untreated WCR. The complex changes and underlying mechanisms require further verification through FTIR spectroscopy analysis.

3.1.4. FTIR spectroscopy

Fig. 9 displays the FTIR spectra of U_C and the six treated samples. Since U_C underwent no cleaning or treatment, its spectrum exhibits numerous small, irregular peaks due to the influence of various complex additives and residual impurities. However, this does not hinder the comparative analysis of key absorption peaks across different spectra. Overall, each treated sample either retained or altered absorption peaks within the corresponding wavenumber ranges to varying degrees, with HHC and SLC exhibiting the most pronounced changes relative to U_C.

The FTIR spectra of the H_2O_2-treated samples exhibit a consistent trend, showing an absorption peak within 3200–3500 cm^{-1}, along with a significant reduction in the absorption peaks related to C═C at 1500–1600 cm^{-1}, particularly in HHC, where the peak nearly disappears. This confirms the introduction of -OH and the cleavage of C═C bonds, further supporting the findings from the contact angle tests, SEM images, and SSA analysis. Additionally, the peaks associated with C-H vibrations of $-CH_2$ and $-CH_3$ in the ranges of 2800–3000 cm^{-1} and 1350–1450 cm^{-1} decrease, particularly in SMC and HMC. This trend is likely attributed to C-C bond cleavage, small molecule loss, and the reconstruction of surface functional groups during oxidation or alkaline treatments. Notably, within 600–1200 cm^{-1}, U_C exhibits not only C-S and S-S absorption peaks associated with crosslinking but also additional peaks related to oxidation products formed after aging. These crosslinking bonds and oxidation products are reduced in HLC, HMC, and HHC, while new oxidation products are introduced, particularly evident in HHC.

In the spectra of NaOH-treated WCR, the SCL shows no significant introduction of -OH groups, yet strong C═O, S═O, S-O, and C-O characteristic peaks appear around 1700 cm^{-1} and in 800–1200 cm^{-1}, indicating the presence of highly polar functional groups. A striking

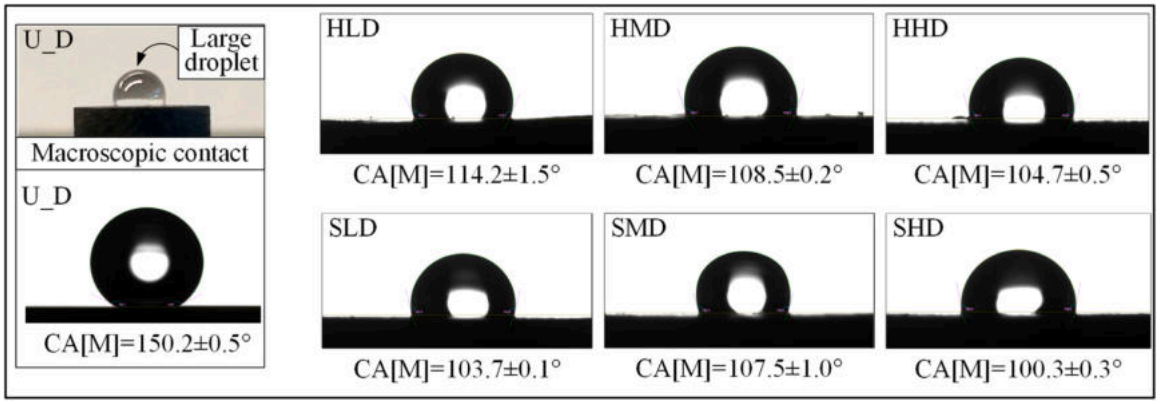

Fig. 8. Contact angle test results.

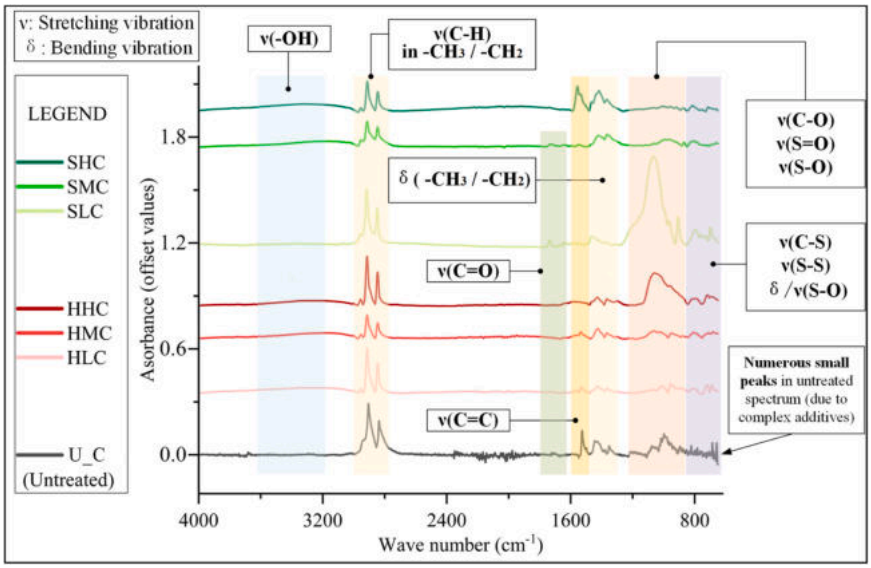

Fig. 9. FTIR spectra for all samples.

observation is that despite undergoing more intense alkaline treatment, SMC and SHC do not exhibit notable absorption peaks associated with sulfur crosslink hydrolysis products. Particularly in SHC, the C═C absorption peak exceeds that of the U_C, which contradicts the typical depletion of unsaturated bonds under alkaline conditions. This anomaly suggests that excessive NaOH-induced degradation may have surpassed the hydrolysis mechanism, instead triggering thermal-alkaline decomposition, as evidenced by degraded WCR residues observed in the waste solution even after dilution in Fig. 11 (a). Under such conditions, both C-S and S-S crosslinks can rupture, producing reactive ·C and ·S radicals. While S-S bond cleavage alone does not generate C═C structures, it disrupts the vulcanized network and induces localized instability, potentially facilitating C-C bond scission. The ·C radicals may subsequently recombine or rearrange into conjugated structures, thus amplifying the C═C signal. Furthermore, the lowest contact angle observed in SHC may partially result from residual NaOH, as high-concentration solutions may leave traces of alkali even after identical washing and drying protocols.

To provide a quantitative comparison, peak areas of characteristic functional groups were calculated from the FTIR spectra, as shown in Table 6. Based on these results, the identified groups were further classified into polar and non-polar categories, and the corresponding ratios were determined for each WCR sample, as illustrated in Fig. 10. This allows a more intuitive assessment of polarity evolution on the WCR surface. Compared to U_C, all treated samples show a reduction in non-polar groups (C-H, C═C) and an increase in polar groups, especially in SLC and HHC, which exhibits the most significant polarity enhancement, consistent with its roughened surface texture and improved wettability. In contrast, SHC and SMC show similar polar-to-nonpolar ratios and the lowest polarity ratios among all the treated samples,

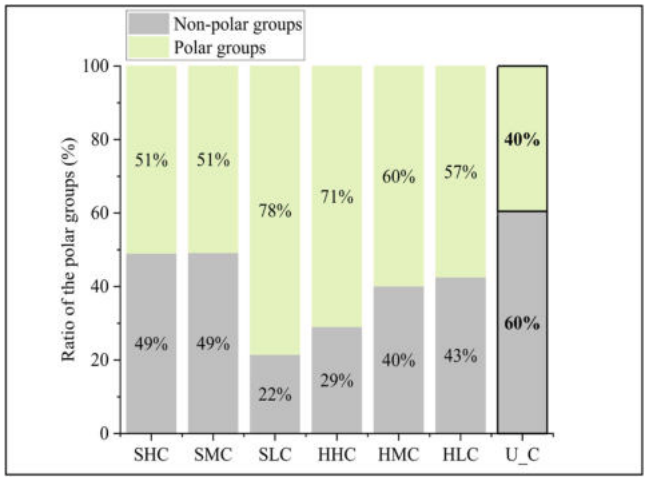

Fig. 10. FTIR results for all samples.

highlighting that excessive treatments yield limited polarity improvement despite harsher conditions.

3.2. Storage stability test

3.2.1. S_{diff}

Table 7 summarizes the S_{diff} between the upper and lower sections of rubberized binder samples after high-temperature storage. According to Yang et al. [37], the surface properties and specific density of WCR are key factors affecting storage stability. Due to weak interfacial

Table 6
Peak areas of the functional groups based on the FTIR spectra (dimensionless).

Samples	Type of functional groups				
	C-H (-CH_3/-CH_2)	C═C	-OH	S═O/S-O/C-O	C═O
SHC	20.902	6.993	20.513	8.434	/
SMC	20.609	0.843	12.899	8.593	0.637
SLC	24.699	/	8.695	80.490	0.882
HHC	18.254	/	12.434	32.047	/
HMC	12.357	2.328	13.813	8.097	/
HLC	17.468	2.115	16.681	9.708	/
U_C	28.809	3.537	2.736	18.417	/

Table 7
Softening point difference between upper and lower sections of the tube (°C).

Samples	Up			Bottom			S_{diff}
	Left	Right	Avg.	Left	Right	Avg.	
HLFB	67.6	67.7	67.7	70.10	70.4	70.3	2.6
HMFB	67.5	67.2	67.4	69.30	69.6	69.5	2.1
HHFB	69.9	69.9	69.9	68.30	67.9	68.1	1.8
SLFB	69.1	69.4	69.3	67.30	67.1	67.2	2.1
SMFB	69.7	69.1	69.4	67.50	66.7	67.1	2.3
SHFB	69.3	69.5	69.4	66.80	67.1	67.0	2.5
U_FB	66.7	67.1	66.9	72.10	72.4	72.3	5.3

interactions between U_FB and bitumen, along with the slightly higher density (1.10 kg/m^3) of U_FB, the system stability is disrupted under the combined effects of temperature and gravity, resulting in S_{diff} exceeding 5 °C.

In contrast, all treated samples showed a significant reduction in S_{diff}, at least halving the value observed in U_FB. HHFB, SLFB, and HMFB exhibited the lowest S_{diff}, indicating the highest system compatibility. HLFB appeared to undergo greater segregation, possibly due to weaker treatment intensity. The greater segregation in SMFB and SHFB is likely a consequence of excessive etching, with potential contributions from residual NaOH shown in Fig. 11 (b). However, the overall differences among treated samples were not substantial, suggesting that both H_2O_2 and NaOH treatments effectively enhanced WCR-bitumen compatibility and reduced phase segregation. This enhancement can be attributed to increased interfacial activity due to improved surface texture, wettability, and chemical properties of treated WCR. Additionally, during the elution process of surface treatment, the detachment of denser precipitates like carbon black was observed, which is consistent with previous findings [15]. This removal led to a decrease in the density of WCR, bringing it closer to that of bitumen. As a result, the gravity-driven relative displacement within the system was mitigated, thereby enhancing the uniformity and overall stability of the material.

Additionally, during the surface treatment process, dark particulate matter was observed, both on the wiped paper and the waste solutions, as shown in Fig. 12 (a), particularly at higher treatment intensities. While direct compositional confirmation was not feasible due to the small and dispersed quantities, several factors support the inference that these particles are carbon black. First, the treatment temperature in this study did not exceed 90 °C, far below the range (160–200 °C) required to thermally degrade vulcanized rubber, as confirmed by previous literature. Therefore, it is unlikely that the particles originate from degraded rubber. Second, carbon black is a common reinforcing filler physically embedded within the WCR network. Surface oxidation and swelling during treatment may partially disrupt the rubber-filler interface, leading to the detachment of some loosely bound particles. Third, Iwase et al. [10] reported that similar dark substances on the oxidized rubber after wiping were identified as detached carbon black, as shown in Fig. 12 (b). These observations also align with those reported by Li et al. [16], further supporting this inference. The density of carbon black is substantially higher than that of the rubber matrix. Therefore, its partial removal during surface treatment leads to a decrease in the overall density of WCR. This narrows the density disparity between WCR and bitumen, which helps mitigate gravity-driven segregation within the modified system and consequently enhances both storage stability and interfacial dispersion.

3.2.2. S_p

Table 8 presents the S_p calculated based on G^* from the DSR temperature sweep test. At both 25 °C and 65 °C, HHFB and SLFB exhibited significantly lower S_p than other samples, indicating the highest phase stability. Additionally, SMFB and SHFB showed similar segregation levels, while HLFB had the highest S_p overall, even exceeding U_FB at 25

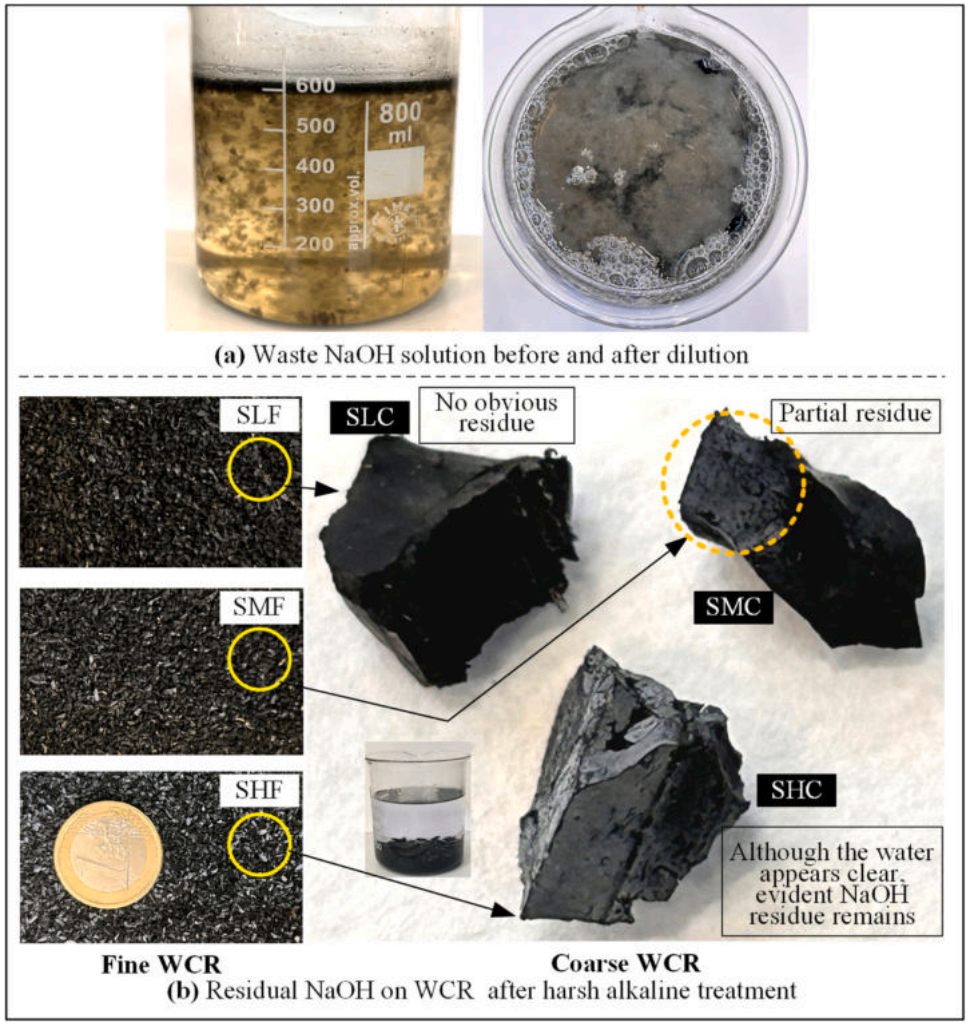

Fig. 11. Degradation and residual on the Surface of WCR after intense NaOH treatment.

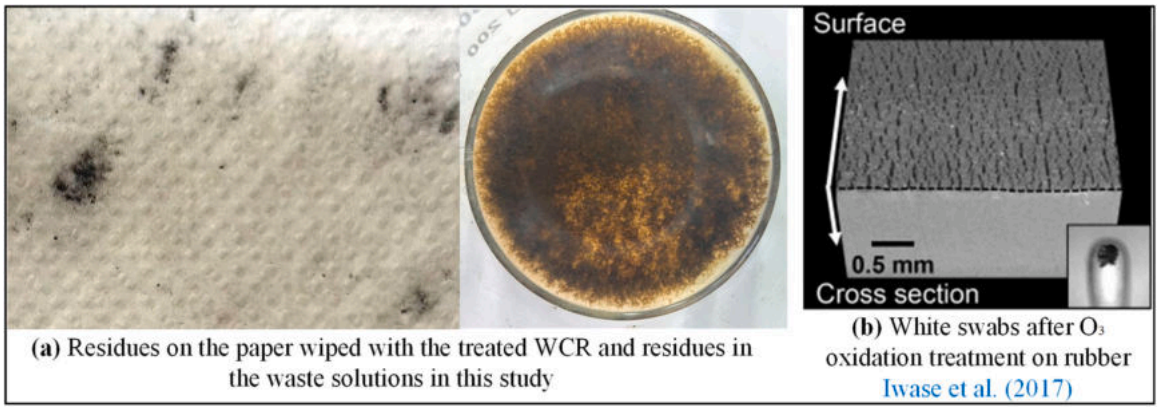

Fig. 12. Residues observed in this study and referenced literature.

Table 8
Segregation rates calculated based on G^*.

Samples	G^* at 25 °C (kPa)				G^* at 60 °C (kPa)			
	Top	Bottom	Avg.	S_p(%)	Top	Bottom	Avg.	S_p(%)
HLFB	1777.3	1264.7	1521.0	16.9	13.101	11.061	12.081	8.4
HMFB	1925.6	1548.5	1737.1	10.9	12.059	9.431	10.745	12.2
HHFB	1712.1	1520.0	1616.1	5.9	14.256	13.194	13.725	3.9
SLFB	1580.3	1419.1	1499.7	5.4	9.591	9.440	9.516	0.8
SMFB	2034.0	1600.6	1817.3	11.9	11.924	10.491	11.208	6.4
SHFB	1677.5	1368.0	1522.8	10.2	11.314	9.912	10.613	6.6
U_FB	1996.9	1653.4	1825.2	9.4	11.915	4.538	8.227	44.8

°C. It should be explained that the S_p of U_FB exceeded 40 % under the 60 °C test condition, which is most likely attributable to a low-probability random error caused by sampling from an already non-uniform specimen. These findings align with the softening point test results. Further analysis, incorporating Fig. 13, compares HHFB and SLFB, the most effective samples, against untreated U_FB.

Fig. 13 (a) shows that as the temperature increases from 15 °C to 35 °C, the phase angles of HHFB, SLFB, and U_FB gradually rise from approximately 42° to 55°. While all three samples exhibit an increasing viscous response, they remain predominantly elastic. Additionally, HHFB and SLFB display nearly identical trends in the viscoelastic behavior of their upper and lower sections, despite not being perfectly overlapping. In contrast, as temperature increases, U_FB exhibits a more pronounced divergence, which is also evident in Fig. 13 (b). From 50 °C to 70 °C, all three samples become more viscous with minimal further variation with continuous increase in temperature, as shown in Fig. 13 (c) and (d). Although this trend differs from low-temperature behavior, U_FB still exhibits greater variation between its upper and lower sections due to phase segregation, compared to HHFB and SLFB.

Interestingly, H_FB exhibits a lower phase angle than S_FB across the temperature sweep in Fig. 13 (a) and (c), indicating a higher elastic contribution in the binder system. This rheological behavior can also be explained by combining SEM images. Under high-temperature conditions, NaOH treatment causes severe structural degradation of WCR, leading to excessive swelling, network loosening, and partial breakdown of crosslinked sulfur bridges. This increases the proportion of soft, low-molecular-weight fragments at the WCR surface, which promotes viscous flow but compromises elastic recoil. Consequently, the resulting binder exhibits reduced elastic response. In contrast, H_2O_2 treatment, though oxidative, induces milder swelling and degradation, better maintaining the crosslinked network, interfacial stiffness, and elastic resistance. This structural preservation ultimately allows more elastic components to be retained and stored during binder preparation.

Fundamentally, H_2O_2 and NaOH treatments enhance the compatibility of WCR with bitumen by introducing polar groups and altering surface morphology. Microscopically, the emergence of polar groups enhances hydrogen bonding and dipole-dipole interactions with bitumen's aromatic and resinous fractions, while surface roughness increases mechanical interlocking. These changes facilitate interfacial wetting and molecular diffusion, enabling deeper penetration of bitumen into the WCR matrix and more effective entanglement at the phase boundary. Consequently, the interphase becomes more continuous and mechanically integrated, reducing mobility mismatch and inhibiting phase separation. This explains the observed improvements in storage stability and rheological uniformity.

3.3. Modified boiling test

Table 9 shows the S_r calculated through the modified boiling test. U_C exhibited the highest bitumen S_r, approaching 50 %, indicating that nearly half of the bitumen adhered to WCR detached after boiling, reflecting weak interfacial adhesion. HLC and SHC showed slightly improved adhesion with bitumen, but their S_r remained relatively high at around 35 %. Samples subjected to moderate treatment intensity, HMC and SMC, the S_r further decreased to around 30 %, indicating more stable WCR-bitumen interfacial bonding. Notably, HHC and SLC demonstrated the lowest S_r values, around 22 %, less than half of that of U_C, representing the strongest bitumen retention. This macroscopic perspective corroborates previous microscopic analyses. Compared to untreated WCR, HHC and SLC exhibit significantly increased surface polarity while maintaining adequate micro-texture. This dual improvement enhances both thermodynamic compatibility and mechanical interlocking. The introduced polar groups enable stronger intermolecular interactions with bitumen, reducing interfacial energy, while the preserved surface roughness promotes capillary infiltration and physical anchoring. Together, these effects stabilize the WCR-bitumen interface against thermal-induced debonding, contributing to improved adhesion durability.

Comprehensively, at H_2O_2 solution below 2 mol/L, higher concentrations and temperatures more significantly enhance the physical and

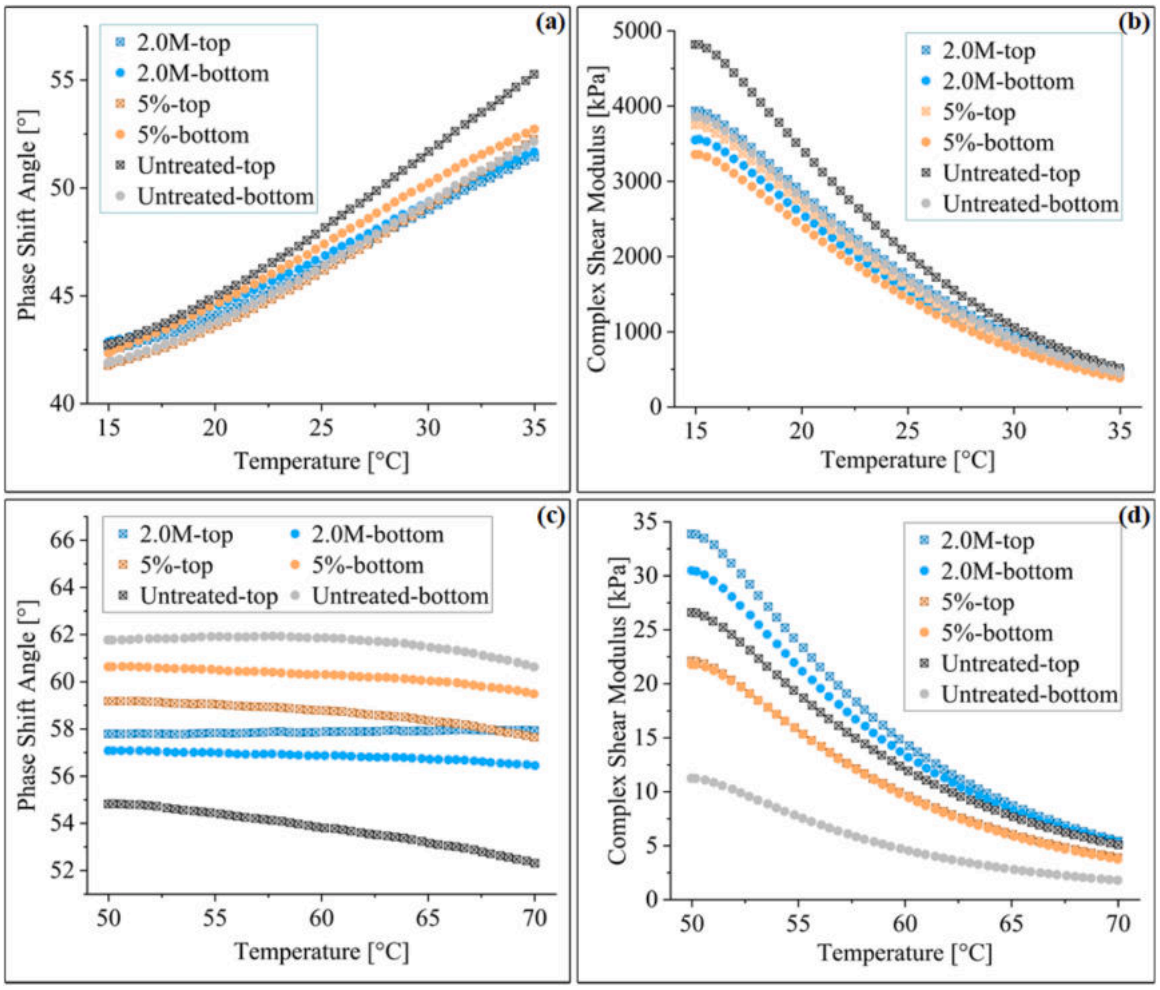

Fig. 13. Phase Angle and Complex Modulus of HHFB, SLFB, and U_FB.

Table 9
Striping rate based on the modified boiling test.

Samples	m_0 (g)	m_1 (g)	m_2 (g)	m_3 (g)	m_1-m_0 (g)	m_3-m_2 (g)	S_r (%)
HLC	50.70	57.94	209.61	212.15	7.24	2.54	35.08
HMC	50.57	58.68	209.61	212.02	8.11	2.41	29.72
HHC	50.54	59.59	209.61	211.59	9.05	1.98	21.88
SLC	50.85	60.05	209.61	211.71	9.20	2.10	22.83
SMC	50.85	59.37	209.61	212.01	8.52	2.40	28.17
SHC	50.93	58.91	209.61	212.27	7.98	2.66	33.33
U_C	50.61	57.76	209.61	213.08	7.15	3.47	48.53

chemical properties of the WCR surface. However, unexpectedly, high-temperature NaOH solutions with concentrations exceeding 15 % did not outperform in improving the WCR-bitumen interfacial compatibility. Fig. 14 provides a summary illustration of how the treatment efficacy of WCR varies with changes in concentration and temperature for both reagents.

It is worth emphasizing that the above findings are insufficient to substantiate the claim that 5 % NaOH at 30 °C represents the optimal treatment condition. Indeed, Nuzaimah et al. [22] have reported superior surface modifications at concentrations below 10 % under more aggressive conditions. While this observation reinforces the notion that, at lower concentrations, the effectiveness of WCR surface treatment is positively correlated with treatment intensity, it also implies that the optimal conditions may instead lie within the range of 10–15 % NaOH and 30–60 °C.

4. Conclusions

This study systematically examined the effects of H_2O_2 and NaOH treatments under varying intensities on WCR surface properties and their impact on WCR-bitumen interfacial compatibility and adhesion. The key findings and conclusions are as follows:

1. Both H_2O_2 and NaOH effectively activate the WCR surface, improving its compatibility with bitumen. This is attributed to oxidation, cleavage, and hydrolysis of C═C, C-C, C-S, and S-S bonds, introducing additional polar functional groups. Consequently, it leads to surface etching and significantly enhances wettability.
2. For H_2O_2, treatment effectiveness improves with increasing concentration and temperature below 2 mol/L. NaOH, however, does not show a clear positive correlation with treatment intensity, as excessive conditions may cause over-etching and reduced cost-efficiency, without necessarily enhancing surface area, roughness, or polarity. Treatments using 10–15 % NaOH at various temperatures deserve further investigation.
3. HHC and SLC exhibit markedly rougher surfaces and an eightfold increase in SSA compared to untreated WCR, with contact angles reduced by one-third and a rise in polar groups, which is further validated by decreased bitumen stripping and binder segregation.
4. SEM and DSR analyses suggest slight swelling under severe treatments, which smooths the surface, promotes the elastic-to-viscous transition, and facilitates the detachment of high-density fillers such as carbon black. This, in turn, reduces the density gap between

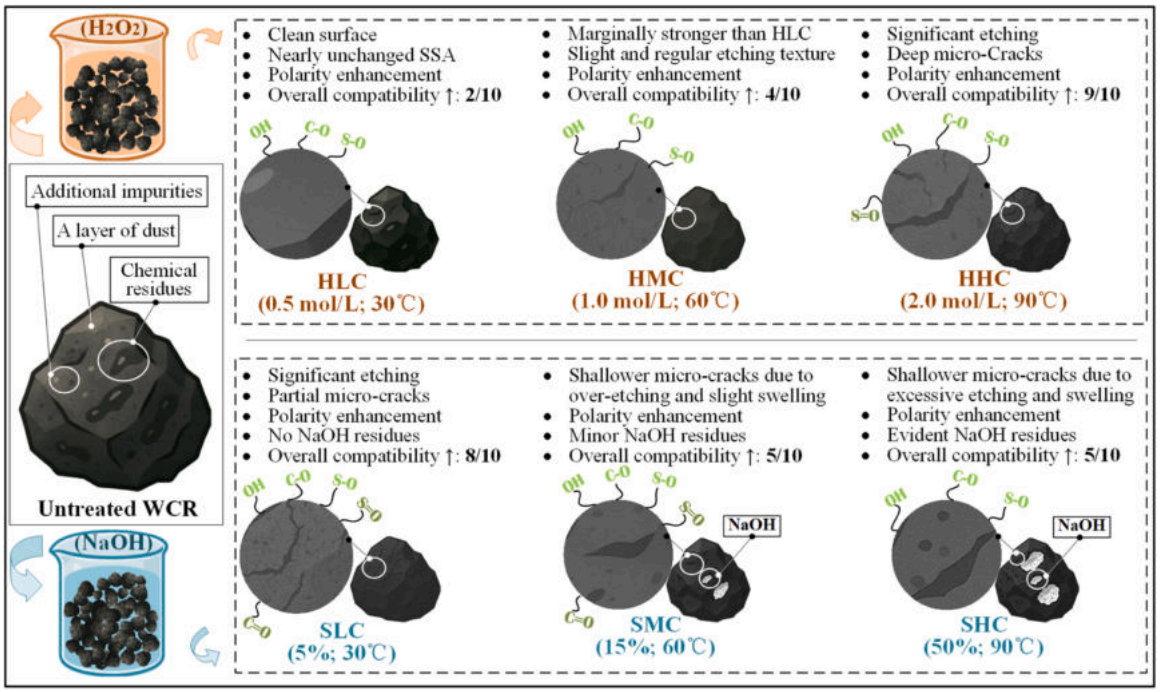

Fig. 14. Effects of different treatments on WCR (schematic).

WCR and bitumen, mitigating gravity-driven segregation and enhancing phase stability.

These findings offer insights into more sustainable WCR surface treatments and provide a practical basis for optimizing experimental conditions. Regardless of wet or dry application, they enhance WCR-bitumen interlocking and bonding, promoting higher recycling efficiency in asphalt pavements. Given the comparable modification efficiency, low residual retention in WCR, and ease of post-treatment waste management, H_2O_2 represents a more recommended approach. Meanwhile, this study primarily focused on the physicochemical changes of WCR and their influence on interfacial compatibility with bitumen. Further research is to evaluate the overall performance of modified binders and mixtures incorporating treated WCR under both wet and dry processes, with particular attention to mechanical properties and durability.

CRediT authorship contribution statement

Piergiorgio Tataranni: Writing – review & editing, Validation, Supervision, Resources, Methodology, Formal analysis, Conceptualization. **Nie Tian:** Writing – review & editing, Writing – original draft, Visualization, Validation, Software, Resources, Methodology, Investigation, Formal analysis, Data curation, Conceptualization. **Cesare Sangiorgi:** Writing – review & editing, Validation, Supervision, Resources, Project administration, Methodology, Funding acquisition, Formal analysis, Conceptualization. **Yinzhang He:** Validation, Software, Resources, Investigation, Formal analysis.

Declaration of Competing Interest

The authors declare that they have no competing financial interests or personal relationships that could have appeared to influence the work reported in this paper.

Acknowledgments

This study was funded by the research project "Green-health-safety Nexus for New Urban spaces - GreeNexUS" (HORIZON MSCA - 2021 DN) Grant Agreement n° 101073437: Research grant under the title "Impact Absorbing Pavements with Improved Accessibility Features (DC9 - IAP)". (https://greenexus.unibo.it/researches/iap/) The authors also appreciate Genan S.A. (Portugal) (https://www.genan.eu/) for providing the waste tire rubber materials used in the pilot study.

Appendix A. Supporting information

Supplementary data associated with this article can be found in the online version at doi:10.1016/j.conbuildmat.2025.142996.

Data Availability

Data will be made available on request.

References

[1] A.A. Aziz, M. Rosli, A.K. Dora, N. Zakaria, N. Jafri, Utilization of sodium hydroxide (Naoh) to treat used tyres as sand partial replacement in engineered cementitious composites, Int. J. Integr. Eng. 14 (9) (2022) 164–170.
[2] C.M. Copetti, P.M. Borges, J.Z. Squiavon, S.R. da Silva, J.J. de Oliveira Andrade, Evaluation of tire rubber surface pre-treatment and silica fume on physical-mechanical behavior and microstructural properties of concrete, J. Clean. Prod. 256 (2020) 120670.
[3] D. Dong, X. Huang, X. Li, L. Zhang, Swelling process of rubber in asphalt and its effect on the structure and properties of rubber and asphalt, Constr. Build. Mater. 29 (2012) 316–322.
[4] A. Farina, M.C. Zanetti, E. Santagata, G.A. Blengini, Life cycle assessment applied to bituminous mixtures containing recycled materials: crumb rubber and reclaimed asphalt pavement, Resour. Conserv. Recycl. 117 (2017) 204–212.
[5] F. Guo, J. Zhang, J. Pei, W. Ma, Z. Hu, Y. Guan, Evaluation of the compatibility between rubber and asphalt based on molecular dynamics simulation, Front. Struct. Civ. Eng. 14 (2020) 435–445.
[6] S. Guo, Q. Dai, R. Si, X. Sun, C. Lu, Evaluation of properties and performance of rubber-modified concrete for recycling of waste scrap tire, J. Clean. Prod. 148 (2017) 681–689.
[7] M. Han, X. Zeng, Y. Muhammad, J. Li, J. Yang, S. Yang, F. Meng, Preparation of octadecyl amine grafted over waste rubber powder (ODA-WRP) and properties of its incorporation in SBS-modified asphalt, Polymers 11 (4) (2019) 665.
[8] N.A. Hassan, A.A.A. Almusawi, M.Z.H. Mahmud, N.A.M. Abdullah, N.A.M. Shukry, N. Mashros, N.I.M. Yusoff, Engineering properties of crumb rubber modified dense-graded asphalt mixtures using dry process, Paper presented IOP Conference Series Earth Environmental Science (2019).

[9] Y. He, Q. Wang, J. Zhang, Y. Li, H. He, G. Huang, Foamed crumb rubber asphalt binder: preparation, rheological properties and adhesion characteristics, J. Clean. Prod. 396 (2023) 136516.
[10] Y. Iwase, T. Shindo, H. Kondo, Y. Ohtake, S. Kawahara, Ozone degradation of vulcanized isoprene rubber as a function of humidity, Polym. Degrad. Stab. 142 (2017) 209–216.
[11] A. Kashani, T.D. Ngo, P. Hemachandra, A. Hajimohammadi, Effects of surface treatments of recycled tyre crumb on cement-rubber bonding in concrete composite foam, Constr. Build. Mater. 171 (2018) 467–473.
[12] Y.C. Khern, S.C. Paul, S.Y. Kong, A.J. Babafemi, V. Anggraini, M.J. Miah, B. Šavija, Impact of chemically treated waste rubber tire aggregates on mechanical, durability and thermal properties of concrete, Front. Mater. 7 (2020) 90.
[13] S. Kocak, M.E. Kutay, Effect of addition of dry crumb rubber on the performance of terminal blend crumb rubber modified asphalt mixtures, Transp. Res. Rec. 2633 (1) (2017) 90–97.
[14] S. Kocak, M.E. Kutay, Use of crumb rubber in lieu of binder grade bumping for mixtures with high percentage of reclaimed asphalt pavement, Road. Mater. Pavement Des. 18 (1) (2017) 116–129.
[15] B. Li, H. Li, Y. Wei, X. Zhang, D. Wei, J. Li, Microscopic properties of hydrogen peroxide activated crumb rubber and its influence on the rheological properties of crumb rubber modified asphalt, Materials 12 (9) (2019) 1434.
[16] B. Li, Y. Wei, Y. Wang, Y. Cui, Effect of hydrogen peroxide treated rubber powder on viscoelasticity of rubber modified asphalt, Acta Mater. Compos. Sin. 36 (2019) 1008–1016.
[17] F. Li, X. Zhang, L. Wang, R. Zhai, The preparation process, service performances and interaction mechanisms of crumb rubber modified asphalt (CRMA) by wet process: a comprehensive review, Constr. Build. Mater. 354 (2022) 129168.
[18] J. Li, Z. Chen, F. Xiao, S.N. Amirkhanian, Surface activation of scrap tire crumb rubber to improve compatibility of rubberized asphalt, Resour. Conserv. Recycl. 169 (2021) 105518.
[19] C. Makoundou, A. Fathollahi, S. Kleiven, S.J. Coupe, C. Sangiorgi, Mechanical and leaching characterisation of impact-absorbing rubberised asphalts for urban pavements, Mater. Struct. 56 (3) (2023) 55.
[20] C. Makoundou, K. Johansson, V. Wallqvist, C. Sangiorgi, Functionalization of crumb rubber surface for the incorporation into asphalt layers of reduced stiffness: an overview of existing treatment approaches, Recycling 6 (1) (2021) 19.
[21] K.B. Najim, M.R. Hall, Crumb rubber aggregate coatings/pre-treatments and their effects on interfacial bonding, air entrapment and fracture toughness in self-compacting rubberised concrete (SCRC), Mater. Struct. 46 (2013) 2029–2043.
[22] M. Nuzaimah, S. Sapuan, R. Nadlene, M. Jawaid, Sodium hydroxide treatment of waste rubber crumb and its effects on properties of unsaturated polyester composites, Appl. Sci. 10 (11) (2020) 3913.
[23] M.M. Phiri, M.J. Phiri, K. Formela, S.P. Hlangothi, Chemical surface etching methods for ground tire rubber as sustainable approach for environmentally-friendly composites development–a review, Composites Part B Engineering 204 (2021) 108429.
[24] A. Riekstins, J. Baumanis, J. Barbars, Laboratory investigation of crumb rubber in dense graded asphalt by wet and dry processes, Constr. Build. Mater. 292 (2021) 123459.
[25] K. Shahzad, Z. Zhao, Experimental study of NaOH pretreated crumb rubber as substitute of fine aggregate in concrete, Constr. Build. Mater. 358 (2022) 129448.
[26] K.M. Shatanawi, S. Biro, M. Naser, S.N. Amirkhanian, Improving the rheological properties of crumb rubber modified binder using hydrogen peroxide, Road. Mater. Pavement Des. 14 (3) (2013) 723–734.
[27] R. Si, S. Guo, Q. Dai, Durability performance of rubberized mortar and concrete with NaOH-Solution treated rubber particles, Constr. Build. Mater. 153 (2017) 496–505.
[28] S. Singh, W. Nimmo, B. Gibbs, P. Williams, Waste tyre rubber as a secondary fuel for power plants, Fuel 88 (12) (2009) 2473–2480.
[29] J. Sun, X. Lv, Y. Zhang, J. Yang, The water stability research of the rubber powder-modified asphalt mixture. Paper presented at the IOP Conference Series: Earth and Environmental Science;2020.
[30] N. Tian, P. Tataranni, C. Sangiorgi, Hydrogen peroxide activation of waste tire crumb rubber for improving compatibility with bitumen: laboratory and molecular dynamics insights, J. Road. Eng. (2025).
[31] V. Torretta, E.C. Rada, M. Ragazzi, E. Trulli, I.A. Istrate, L.I. Cioca, Treatment and disposal of tyres: two EU approaches. A review, Waste Manag. 45 (2015) 152–160.
[32] H. Wang, X. Liu, P. Apostolidis, S. Erkens, A. Skarpas, Experimental investigation of rubber swelling in bitumen, Transp. Res. Rec. 2674 (2) (2020) 203–212.
[33] X. Wang, L. Hong, H. Wu, H. Liu, D. Jia, Grafting waste rubber powder and its application in asphalt, Constr. Build. Mater. 271 (2021) 121881.
[34] C. Xiaowei, H. Sheng, G. Xiaoyang, D. Wenhui, Crumb waste tire rubber surface modification by plasma polymerization of ethanol and its application on oil-well cement, Appl. Surf. Sci. 409 (2017) 325–342.
[35] J. Xie, Y. Yang, S. Lv, X. Peng, Y. Zhang, Investigation on preparation process and storage stability of modified asphalt binder by grafting activated crumb rubber, Materials 12 (12) (2019) 2014.
[36] J. Xie, Y. Zhang, Y. Yang, Study on preparation method of terminal blend rubberized asphalt binder, Front. Mater. 7 (2020) 279.
[37] X. Yang, Z. Ning, X. Feng, X. He, S. Tan, Methods for improving storage stability of rubber bitumen: a review, J. Clean. Prod. (2024) 141595.
[38] H. Yaqoob, Y.H. Teoh, F. Sher, M.A. Jamil, D. Murtaza, M. Al Qubeissi, M. Mujtaba, Current status and potential of tire pyrolysis oil production as an alternative fuel in developing countries, Sustainability 13 (6) (2021) 3214.
[39] K. Yu, H. Wang, H. Han, R. Li, X. Chen, J. Du, S. Liu, Hydrogen peroxide oxidizing modification of crumb tire rubber and its application in modified bitumen, J. Tianjin Univ. Sci. Technol. 47 (2014) 949–954.
[40] S. Yu, F. Chen, D. Hu, D. Cao, C. Liu, Q. Wang, N. Yalikun, Effect of hydrogen peroxide oxidation waste rubber powder on asphalt compatibility, Constr. Build. Mater. 453 (2024) 139074.
[41] J.L. Zhang, H.X. Chen, C.M. Ke, Y. Zhou, H.Z. Lu, D.L. Wang, Graft polymerization of styrene onto waste rubber powder and surface characterization of graft copolymer, Polym. Bull. 68 (2012) 789–801.

Nie Tian, a Ph.D. candidate and Marie Curie Fellow at the Department of Civil, Chemical, Environmental, and Materials Engineering (DICAM), University of Bologna, Italy, is currently focusing on relevant research about "Impact Absorbing Pavements (IAP) with Improved Accessibility Features." Her broader interests include innovative pavement materials, cold paving and repair techniques, and life cycle assessment of pavement materials.

Piergiorgio Tataranni is a post-doc research fellow (junior assistant professor-fixed-term) in the Department of Civil, Chemical, Environmental and Materials Engineering at the Alma Mater Studiorum-University of Bologna. Since 2013, his activity in the roads section of the department has focused on themes related to pavement materials and construction technologies for civil infrastructures. His research is mainly centred on the development of innovative and sustainable materials and low-impact construction technologies. On these topics, he is the author of several scientific publications, his PhD thesis, and he participated in European projects as an early-stage researcher (H2020, REMINE, MSCA-RISE-2014) and scientific manager (SAFERUP! H2020 MSCA ITN-2017). https://www.unibo.it/sitoweb/piergiorg.tataranni2/

Yinzhang He received the B.S. degree in road, bridge, and river-crossing engineering from Wuhan Institute of Technology in 2020. He is currently pursuing a Ph.D. degree in highway and railway engineering at Chang'an University. His research interests include intelligent inspection and repair and maintenance technologies for airport pavements, with a special focus on the use of big data and distress identification algorithms for airport pavements.

Cesare Sangiorgi is a full professor at the Alma Mater Studiorum- University of Bologna. He specializes in pavement engineering materials and sustainable construction technologies, prioritizing recycled materials and low-impact solutions. He fosters student engagement through collaborations with esteemed research institutes. Since 2001, he's partnered with the Nottingham Transportation Engineering Centre and expanded collaborations globally. He led SAFERUP! recruiting 15 early-stage researchers in a consortium of 30 for sustainable urban pavement projects. Presently, he coordinates GreeNexUS, a HORIZON EUROPE project promoting urban greening and infrastructure safety. With numerous research agreements nationally and internationally, he actively contributes to professional associations like SIIV, APSE, iSMARTi, and RILEM, and serves on journal boards and conference committees, publishing extensively in pavement engineering. https://www.unibo.it/sitoweb/cesare.sangiorgi4/